Nuclear Engineering and Technology xxx (xxxx) xxx

Contents lists available at ScienceDirect

Nuclear Engineering and Technology

journal homepage: www.elsevier.com/locate/net

Original Article

Comparison of two kinetic approaches for modeling of radial hydride fraction in zirconium-based fuel rod cladding

Mikhail Kolesnik

Institute for Applied Materials, Karlsruhe Institute of Technology, Karlsruhe, Germany

ARTICLE INFO

Keywords:
Hydride embrittlement
Reorientation of hydrides
Zirconium cladding
Nuclear fuel

ABSTRACT

Theoretical models simulating the kinetics of the radial hydride fraction in the zirconium cladding of fuel rods are developed to predict their hydride embrittlement degree and to justify the safety regimes for the storage and handling of spent nuclear fuel. Currently, there are a number of kinetic models based on different assumptions, approximations and experimental datasets used for their verification. These models can be divided into two groups according to the assumption on how they define the radial hydride fraction f_r precipitated at the current time step: directly from physically based equations (Approach 1) or through engineering correlations for the cumulative radial hydride fraction (Approach 2). The present study investigates the effect of this single assumption on the simulation results of kinetic models. It is shown that Approach 1 assumes a higher relative role for hydrides precipitated at low temperatures than Approach 2 in its current form.

1. Introduction

Spent nuclear fuel (SNF) from nuclear power plants cannot currently be fully recycled without producing high-level radioactive waste. Therefore, spent fuel assemblies are typically stored for several decades to reduce their radioactivity. Dry storage (DS) is a widely used technology for SNF storage. In DS, spent fuel assemblies are placed in hermetically sealed containers filled with an inert gas or a gas that prevents corrosion. The storage conditions must ensure the structural integrity, hermetic state, and necessary level of ductility of fuel rod cladding throughout the entire storage period. Hydride embrittlement of zirconium alloys is one of the most dangerous physical processes that can cause embrittlement of fuel rod cladding in DS conditions and poses a risk to nuclear safety [1].

Zirconium-based alloys are commonly used in the nuclear industry as the fuel rod cladding material in water-cooled nuclear reactors. Hydrogen is picked up by the metal during operation as a secondary product of water corrosion and forms a hydride phase when its concentration exceeds the solubility limit. The presence of hydrides in zirconium alloys reduces ductility and can change the primary fracture mode from ductile to brittle [2]. There are several mechanisms by which hydrides can influence the processes of crack nucleation and growth. Hydrides can serve as preferential fracture nucleation sites, provide a path for brittle cracks with minimal fracture energy through the sample, and increase the inhomogeneity of the ductile flow in the metal. The necessary condition for brittle fracture at the stress level typical to SNF DS is percolation of the brittle crack, i.e. the hydride morphology must be able to provide the path for the brittle crack through the thickness of the specimen [2].

The morphology of hydrides is determined by thermomechanical conditions during precipitation. After the fuel operation, when the fuel assembly is in the fuel pool at low temperatures around 50 °C, the hydrides in the fuel rod cladding are predominantly oriented in the circumferential direction. However, at the beginning of DS and/or during vacuum drying prior to DS, the cladding temperature growth due to the after-power heat production in the fuel composition and can exceed 350–400 °C. This leads to the dissolution of a substantial part or even all the hydrides, which then precipitate again during the subsequent temperature reduction as the after-power heat production naturally decreases with time. During cooling, the gas pressure inside the cladding exceeds the gas pressure in the sealed container, generating tensile circumferential stresses in the fuel rod cladding. This loading scheme can lead to the precipitation of radially-oriented hydrides. Radial hydrides can provide an easy path for brittle crack growth in the radial direction through the cladding thickness and therefore pose a much higher risk of embrittlement than the circumferential ones. The change in orientation of hydrides before and after the thermomechanical cycle due to their dissolution and reprecipitation is known as hydride reorientation.

Hydride reorientation is typically studied through experiments involving thermomechanical cycles that simulate DS conditions. These experiments include partial or total dissolution of hydrides during heating and holding at maximum temperature, followed by their reprecipitation during cooling under different external stresses. The morphology of the hydrides is measured after the test as a cumulative result of the entire thermal cycle. The result of such experiments is the

https://doi.org/10.1016/j.net.2025.103479
Received 15 May 2024; Received in revised form 30 December 2024; Accepted 15 January 2025
Available online 18 January 2025

Please cite this article as: Mikhail Kolesnik, *Nuclear Engineering and Technology,* https://doi.org/10.1016/j.net.2025.103479

reorientation curve: dependence of radial hydride fraction (RHF) on external stresses which is a threshold function, as it can be seen in Fig. 2. The orientation of hydrides at low stresses is determined by the texture and microstructure of the sample [3,4]. At low stresses below the lower threshold stresses, RHF has a weak dependence on external stresses. However, if the stresses exceed the lower threshold, RHF grows rapidly until complete reorientation, which occurs at an upper threshold stress, as shown in Fig. 2. Stress thresholds are parameters of a reorientation curve and characterize the material behavior under the conditions of the particular reorientation test.

Experiments alone are not sufficient to justify the safety of SNF DS conditions, as they cannot cover all possible combinations of factors influencing the hydride morphology at the end of DS. These factors include the initial chemical composition and metallurgical state of the alloy, its irradiation history and final burn-up, oxide thickness, hydrogen content and fuel rod internal gas pressure at the end of operation, as well as the maximum temperature during DS and preceding drying, cooling rate, possible thermal cycling, thermal and stress gradients, and others. The assessment of the hydride morphology in a specific fuel rod and a specific thermomechanical scenario is solved by simulation using theoretical approaches. The parameters influencing the hydride morphology and the type of corresponding dependence used in these approaches must be physically based and experimentally verified. Engineering correlations may fail to describe hydride morphology outside the range of experimental conditions in which they have been verified, whereas the physically based models are expected to be much more reliable for this purpose. Typically, hydride reorientation models simulate the kinetics of hydrogen in solid solution, radial and circumferential hydrides during thermomechanical treatment and the reorientation curves. Currently, there are two popular approaches developed for these purposes in the nuclear industry.

The paper is structured as follows. Section 2 describes the basic assumptions of the kinetic models, which are divided into two groups called “Approach 1″ and “Approach 2". The affiliation of an individual model to a particular approach is defined by an assumption about the nature of the instantaneous radial hydride fraction function. The paper does not compare specific published models, but examines the pure effect of this single assumption and uses unified representative “basic” models to compare the approaches. The “basic” models differ only in the assumption about the type of the instantaneous radial hydride fraction function (all secondary assumptions, material parameters and verification dataset are the same) and are described in Section 3. In Section 4, I compare the approaches with published experimental data. Section 5 is dedicated to thermomechanical scenarios where the approaches exhibit divergence. And in Section 6, I investigate the effect of the approach on the calculation result of dry storage conditions.

2. Description of approaches

The main parameter simulated in hydride reorientation models is the cumulative radial hydride fraction (RHF), or F_r, which is defined as:

$$F_r = \frac{C_r}{C_h} \tag{1}$$

C_r – hydrogen concentration in radial hydrides, C_h – total hydrogen concentration in the hydride phase; $C_h = C_r + C_c$, where C_c is the hydrogen concentration in circumferential hydrides.

In a typical experimental thermomechanical cycle, the value of the $F_r(t)$ function is not normally measured during the experiment, except its value at the final time point $F_r(t_{end})$, where it can be measured directly as a result of microstructural analysis. In non-kinetic hydride reorientation models $F_r(t_{end})$ can be approximated by correlations based on physical equations [5–7], or an engineering polyline function [8] as a function of the parameters of the cycle (e.g. maximum temperature, hydrogen content and stress level for a given stress history, etc.).

Kinetic models operate with the instantaneous fraction of radially-oriented hydrides, or f_r, which is defined as the fraction of hydrides at the current time step that are precipitated as a part of radially-oriented hydrides:

$$f_r = \frac{\mathrm{d}C_r}{\mathrm{d}C_h} \tag{2}$$

As it can be seen from Eqs. (1) and (2), the functions f_r and F_r are related as follows:

$$f_r \cdot \mathrm{d}C_h = \mathrm{d}(F_r \cdot C_h) \tag{3}$$

Therefore, if one function f_r or F_r is defined, the other can also be determined by Eq. (3). There are two approaches used in published kinetic models to define f_r: directly from physically based equations and through engineering correlations for F_r.

2.1. Approach 1 (direct definition of f_r from physically based equations)

The main assumption of the Approach 1 is based on the results of microstructural studies of hydrides, which demonstrate that the macroscale hydrides (tens and hundreds of micrometers hydrides), known as “stacks”, are composed of microscale hydrides (with lengths below a few micrometers), e.g. Ref. [9]. This can be interpreted to mean that the growth of the stacks during cooling is associated with the continued nucleation of new microscale hydrides. Following this assumption, the fraction of hydrogen precipitated as part of radially oriented stacks at each time step during cooling is determined by the ratio of the nucleation frequencies of microscale hydrides within radial and circumferential stacks. The nucleation frequency of a new phase particle is a well-known function from classical nucleation theory:

$$R \sim Z j_n \cdot \exp(-\Delta G_n / kT) \tag{4}$$

R – nucleation frequency (number of nucleated hydrides per second in a unit volume), Z – Zeldovich factor, j_n – hydrogen flow to a nucleus with a critical size, ΔG_n – Gibbs free energy change, k – Boltzman constant, T – temperature.

The instantaneous fraction of radially oriented hydrides is assumed to be the ratio of the nucleation frequency of radially oriented hydrides to a nucleation frequency of all hydrides (sum of radial and circumferential orientations):

$$f_{r1} = \frac{R_r}{R_r + R_c} = \frac{1}{1 + f_0 \cdot \exp\left(-\frac{\Delta G_{n,c} - \Delta G_{n,r}}{kT}\right)} \tag{5}$$

The next assumption is that the difference in Gibbs free energy changes is a linear function of external tension σ:

$$\Delta G_{n,c} - \Delta G_{n,r} = \sigma \cdot \Delta\Omega \tag{6}$$

The polynomial representation of the function $\Delta G_{n,c} - \Delta G_{n,r}$ was selected to minimize the number of model parameters and assumptions required for calculations. The polynomial of the first degree requires the minimal number of parameters to simulate the reorientation of hydrides with sufficient accuracy.

Substituting Eq. (6) into Eq. (5) gives the basic equation for instantaneous fraction of radially oriented hydrides [10–12]:

$$f_{r1}(\sigma / T) = \frac{1}{1 + f_0 \cdot \exp\left(-\frac{\sigma \cdot \Delta\Omega}{kT}\right)} \tag{7}$$

Kinetic models [11,12] consider F_{r1} as a model variable and define the kinetic equation for F_{r1} from Eq. (3):

$$\frac{dF_{r1}}{dt} = \frac{f_{r1} - F_{r1}}{C_h} \cdot \frac{dC_h}{dt} \tag{8}$$

where f_{r1} is according to Eq. (7).

2.2. Approach 2 (definition of f_r through engineering correlations for F_r)

Approach 2 has been developed in the opposite direction. The main idea is to define the F_r function as an engineering correlation and then determining the f_r through F_r (for example this could be done through Eq. (3)). In a number of published kinetic models [13–16], the F_{r2} after the thermomechanical cycle at $t = t_{end}$ is approximated as a polyline function:

$$F_{r2}(t_{end}) = \begin{cases} 0, \sigma_{thm} \le \sigma_{th,0\%} \\ \dfrac{\sigma_{tmc} - \sigma_{th,0\%}}{\sigma_{th,100\%} - \sigma_{th,0\%}}, \sigma_{th,0\%} \le \sigma_{tmc} \le \sigma_{th,100\%} \\ 1, \sigma_{tmc} \ge \sigma_{th,100\%} \end{cases} \tag{9}$$

where σ_{tmc} – stress level in a thermomechanical cycle (usually, stresses in a cycle with constant external stresses). The hydride reorientation stress thresholds $\sigma_{th,0\ \%}$ and $\sigma_{th,100\ \%}$ in Eq. (9) are model parameters, that can be postulated as constants [14], or as the following correlations on parameters of the thermomechanical cycle [13,15,16]:

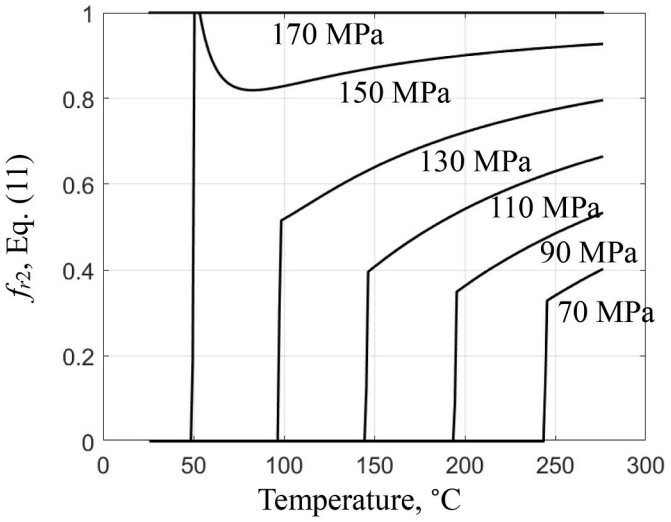

Fig. 1. The instantaneous fraction of radial hydrides (for the current step) according to model [13] (Approach 2) during cooling of samples with 100 ppm from 350 °C at constant stresses.

$$\begin{aligned} &\sigma_{th,0\%}(T_{\max}, C_{tot}) = 0.02 \cdot C_{tot}(\text{wppm}) + 186.9 - 0.3862 \cdot \min\left(T_{\max}\left({}^0C\right), T_{ssd}\left({}^0C\right)\right), [\text{MPa}] \\ &\sigma_{th,100\%}(C_{tot}) = 110 + 65 \cdot (1 - \exp(-C_{tot}(\text{wppm})/65)) \pm 20, [\text{MPa}] \end{aligned} \tag{10}$$

T_{max} – maximal temperature of the thermomechanical cycle, C_{tot} – total hydrogen content, T_{ssd} – temperature of complete hydride dissolution (the function of C_{tot}). The correlations in Eq. (10) have been developed for unirradiated SRA Zircaloy-4 with time-constant and spatially non-uniform stresses during cooling [8].

In the kinetic model [13], f_{r2} is defined by $F_{r2}(t_{end})$ from Eq. (9) as:

$$f_{r2} = \frac{\partial\left(F_{r2}(t_{end}) \cdot C_p\right)}{\partial C_p} = F_{r2}(t_{end}) + C_p \cdot \frac{\partial F_{r2}(t_{end})}{\partial C_p} = F_{r2}(t_{end}) + C_p \cdot \frac{\partial F_{r2}(t_{end})}{\partial T} \Big/ \frac{\partial C_p}{\partial T} \tag{11}$$

where C_p is the hydrogen solubility for precipitation in zirconium.

Eq. (11) contradicts to Eq. (3). The main difference is that instead of the function $F_r(\sigma(t), T(t) \ldots)$ on instantaneous parameters σ, T, (or other possible parameters), the authors of [13] apply the engineering correlation for RHF in the end of the thermomechanical cycle $F_{r2}(t_{end}, \sigma_{tmc}, C_{tot}, T_{ssd})$ on parameters of the corresponding cycle σ_{tmc}, C_{tot}, T_{ssd}, which in Ref. [13] are understood as instantaneous stress $\sigma(t)$, solubility for precipitation at the instantaneous temperature $C_p(T(t))$ and its dissolution temperature $T_{ssd}(C_p(T(t)))$. This discrepancy leads to an artefact of the model: the instantaneous f_{r2} defined by Eq. (11) is a discontinuous function during cooling at constant stresses, as it can be seen in Fig. 1. This discontinuity is the consequence of the differentiation of the non-smooth polyline function $F_{r2}(t_{end})$ in the second term of Eq. (11). The physical meaning of such discontinuity is equivalent to the assumption that hydrides with two different orientations could precipitate under the same conditions (at the point of discontinuity), which has no experimental or theoretical physical confirmation. This artefact of the model [13] is the reason why it is not analyzed further in this study (however, experimental data from the paper [13] play an important role in the comparison of the two approaches below in Section 4.2).

The model [15] uses an alternative relationship to define the f_{r2} function through Eq. (9):

$$f_{r2}(\sigma(t)) = F_{r2}(t_{end}, \sigma_{tmc} = \sigma(t)) \tag{12}$$

The authors of [15] also understand σ_{tmc} in Eq. (9) (stress level in the thermomechanical cycle, applied to determine the correlation for $F_{r2}(t_{end})$) as the instantaneous stress at the current time step in their kinetic extension. Besides, Eq. (12) generally contradicts to Eq. (3). Nevertheless, it has no obvious artefacts and Eq. (12) is considered here as an additional assumption of the model [15], which is currently the most representative of the Approach 2.

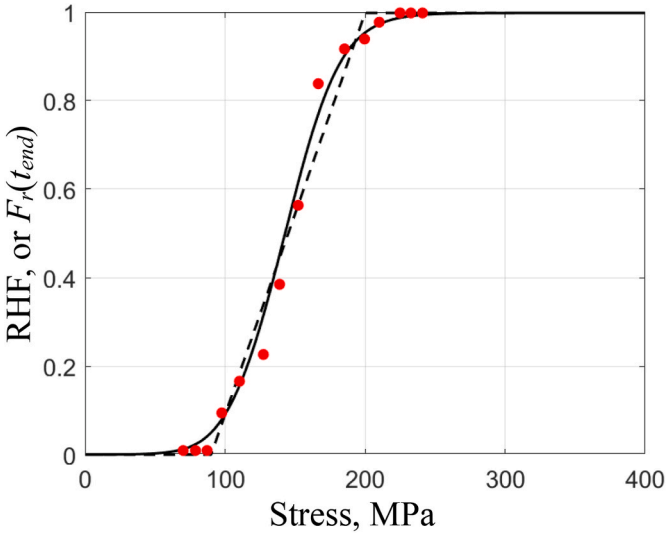

Fig. 2. Cumulative fraction of reoriented hydrides after a thermomechanical cycle with T_{max} = 400 C and 100 ppm; solid line – Approach 1, dashed line – Approach 2, markers – experimental data [6], Zr-2.5Nb.

3. "Basic" models used for simulations in this paper

All the kinetic models cited in Section 2 can be divided into two groups, depending on the assumptions made to determine the f_r function. The aim of this study is to investigate a pure effect of the choice between these two alternatives. However, all the individual models differ in many other aspects which may blur the effect of this single assumption. These differences include non-uniform secondary assumptions, different kinetic approximations, numerical schemes, correlations for hydrogen solubility and experimental datasets used for validation of model parameters. In order to avoid all these removable differences and to make the comparison of approaches (i.e. two assumptions) more precise, the paper uses representative unified "basic" models. The only difference between the "basic" models is the type of the instantaneous radial hydride fraction function f_r.

The simulation of hydrogen kinetics in "basic" models is based on the equation $dC_r = -f_r \cdot dC_s$, where C_s is the hydrogen concentration in solid solution (the same is used in models [10–12], of the Approach 1 and model [15] of the Approach 2). There are two kinetic approximations of "basic" models: quasi-static and diffusion. In both approaches there are three model variables: hydrogen concentration in solid solution ($C_s = C_{tot} - C_h$), radial (C_r) and circumferential (C_c) hydrides. The equilibrium solubility is different for dissolution (TSSD) and precipitation (TSSP), which is known as solubility hysteresis.

The kinetics of hydrogen concentrations in quasi-static approximation is written as:

$$\text{Dissolution}, T < T_{SSD}, C_s \le C_d \quad \text{Precipitation}, T > T_{SSP}, C_s \ge C_p$$

$$\begin{cases} \dfrac{dC_s}{dt} = \dfrac{dC_d}{dt} \\ \dfrac{dC_r}{dt} = -\dfrac{C_r}{C_r + C_c} \cdot \dfrac{dC_s}{dt} \\ \dfrac{dC_c}{dt} = -\dfrac{C_c}{C_r + C_c} \cdot \dfrac{dC_s}{dt} \end{cases} \quad \begin{cases} \dfrac{dC_s}{dt} = \dfrac{dC_p}{dt} \\ \dfrac{dC_r}{dt} = -f_r \cdot \dfrac{dC_s}{dt} \\ \dfrac{dC_c}{dt} = -(1 - f_r) \cdot \dfrac{dC_s}{dt} \end{cases} \tag{13}$$

T_{SSD}, T_{SSP} – temperatures of total dissolution and onset of precipitation; C_d and C_p – solubilities TSSD and TSSP (Arrhenius type functions of temperature).

In diffusional approximation the kinetics of hydrogen is as follows:

$$\text{Dissolution}, T < T_{TSSD}, C_s \le C_d \quad \text{Precipitation}, T > T_{TSSP}, C_s \ge C_p$$

$$\begin{cases} \dfrac{dC_s}{dt} = \dfrac{C_d - C_s}{\tau_0} \\ \dfrac{dC_r}{dt} = -\dfrac{C_r}{C_r + C_c} \cdot \dfrac{dC_s}{dt} \\ \dfrac{dC_c}{dt} = -\dfrac{C_c}{C_r + C_c} \cdot \dfrac{dC_s}{dt} \end{cases} \quad \begin{cases} \dfrac{dC_s}{dt} = \dfrac{C_p - C_s}{\tau_0} \\ \dfrac{dC_r}{dt} = -f_r \cdot \dfrac{dC_s}{dt} \\ \dfrac{dC_c}{dt} = -(1 - f_r) \cdot \dfrac{dC_s}{dt} \end{cases} \tag{14}$$

τ_0 – characteristic diffusion time, which can be estimated as in Ref. [12]:

$$\tau_0 = \frac{l^2}{\alpha^2 D_H} \tag{15}$$

where l – distance between hydrides, α – geometry factor, D_H – diffusion coefficient.

The only difference between the two "basic" models is the interpretation of the f_r function: Approach 1 assumes $f_r = f_{r1}$ according to Eq. (7), while Approach 2 assumes $f_r = f_{r2}$ according to Eq. (12), where the lower and upper thresholds are postulated to be constants (constant thresholds have been also assumed in Ref. [14]). The system Eqs. (13) and (14) are solved numerically using the explicit scheme.

The parameters of the "basic" models have been unified as far as possible for both approaches. The main unavoidable difference is that the reorientation susceptibility of hydrides is characterized by stress thresholds in Approach 2. However, in Approach 1 the thresholds are not considered as material constants, but as characteristics of a reorientation curve, which depends on both material properties and parameters of the thermomechanical cycle. In order to minimize the differences in the approaches, the model parameters of the "basic" models have been verified on the same set of experimental data. The corresponding experiments and the comparison with the simulation results are presented and discussed in Section 4.1. The values of the model parameters used in the simulations in this paper are summarized in Table 1.

4. Comparison with experiments

4.1. Simulation of the reorientation curve (constant stresses)

Both approaches can accurately describe the reorientation curve (dependence of RHF on external stresses) at the end of a single thermomechanical cycle. This can be seen in Fig. 2, which compares the simulation results of quasi-static models of both approaches with the reorientation experiments [6]. The corresponding samples in Ref. [6] were Zr-2.5Nb plates hydrogenated up to 100 ppm and subjected to a

Table 1
Values of the model parameters used in the calculations in this paper.

Alloy	Approach	Parameter	Value	Unit	Reference
SRA Zircaloy-4	1	f_0	10^2	–	Based on [13,17,18]
		$\Delta\Omega$	$2.3 \cdot 10^{-28}$	m^3	
	2	$\sigma_{th,0\ \%}$	70	MPa	
		$\sigma_{th,100\ \%}$	210	MPa	
	Both	C_d	$1.28 \cdot 10^5 \cdot \exp(-36540/RT)$	ppm	[13,19]
		C_p	$6.91 \cdot 10^4 \cdot \exp(-29900/RT)$	ppm	[13,20]
Zr-2.5Nb	1	f_0	10^4	–	Based on [6]
		$\Delta\Omega$	$4.34 \cdot 10^{-28}$	m^3	
	2	$\sigma_{th,0\ \%}$	90	MPa	
		$\sigma_{th,100\ \%}$	200	MPa	
	Both	C_d	$4.4 \cdot 10^5 \cdot \exp(-44606/RT)$	ppm	[21]
		C_p	$2.473 \cdot 10^4 \cdot \exp(-25840/RT)$	ppm	[22]
Zr-based	Both	l	100	mkm	–
		α	0.5	–	[12]
		D_H	$7.73 \cdot 10^{-7} \cdot \exp(-5360/T)$	$m^{-2} \cdot s^{-1}$	[23]

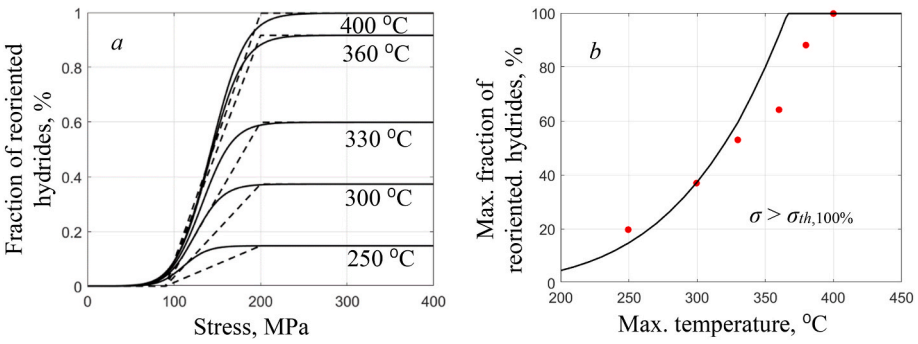

Fig. 3. Reorientation curves at different maximum temperatures ($C_{H,tot}$ = 100 ppm) solid lines – Approach 1, dashed lines – Approach 2, markers – experimental data [6], Zr-2.5Nb.

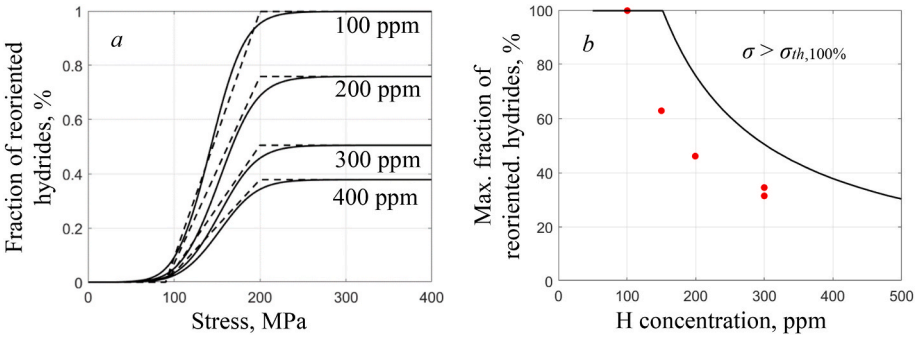

Fig. 4. Reorientation curves at different hydrogen concentrations (T_{max} = 400 °C) solid lines – Approach 1, dashed lines – Approach 2, markers – experimental data [6], Zr-2.5Nb.

Table 2
Comparison of simulation results of "basic" models with experimental data on hydride reorientation in tests with unirradiated SRA or CWSR Zircaloy-4 under time constant and spatially uniform stresses during cooling.

ref.	Conditions			Exp. Value	Approach 1, "basic"	Approach 2, "basic"
	H, ppm	T_{max}, °C	σ, MPa			
[18]	270	400	–	$\sigma_{th,0\ \%}$ = 75 MPa	~64–87 MPa (RHF = 5–10 %)	70 MPa (postulated)
[13] test 7	156	350	110	RHF = 25 ± 4.7 %	22 %	20 %
[17] 1 cycle	250	400	160	RHF = 35–57 %	45 %	48 %

thermomechanical cycle with maximum temperature of 400 °C under constant stress. Hydrogen concentration and maximum temperature were varied in other series of experiments in Ref. [6]. The maximum fraction of reoriented hydrides in these tests decreases with decreasing maximum temperature and increasing hydrogen content, Figs. 3 and 4. This is a consequence of incomplete hydride dissolution, as undissolved hydrides retain their orientation after thermomechanical treatment. Both approaches reproduce the main features of the reorientation curve and its dependence on the parameters of the thermomechanical cycle. The accuracy of the simulation for conditions in Figs. 3 and 4 is determined in a great extent by the accuracy of the solubility and is almost the same for both approaches.

Experiments [6] on Zr-2.5Nb reconstruct the detailed reorientation curves and help to visualize the differences between the approaches in Fig. 2: smooth reorientation curve resulting from Approach 1 and polyline resulting from Approach 2. For SRA Zircaloy-4 the analogue experiments reconstructing the full reorientation curve have not yet

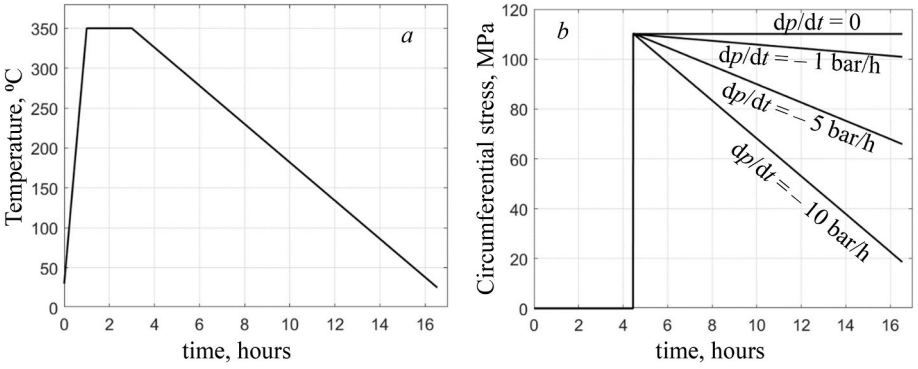

Fig. 5. Temperature and stress histories in experiments [13].

been published. Therefore, to verify the model parameters for the "basic" models for SRA Zircaloy-4, the few reference points from different experiments were used, which are summarized in Table 2. All experiments have been carried out with gas filled tubular unirradiated specimens, generating time constant and spatially uniform stresses during cooling; the hydrogen concentration is close to the solubility for dissolution at maximum temperature. This was done in order to calibrate the parameters of the "basic" models in the same tests with constant stresses during cooling and then to compare the dependencies of RHF on stress reduction rate with the highest possible accuracy, but only within a narrow range of conditions (temperature, hydrogen content, loading scheme) relevant to the experiment [13] (more details in Section 4.2).

4.2. Dependence of RHF on stress reduction rate during cooling

The samples used in the experiment [13] were gas-filled tubes made of SRA Zircaloy-4 and hydrogenated to 100 and 150 ppm. They were subjected to a thermomechanical cycle with a maximum temperature of 350 °C, at which the hydrogen solubility TSSD is about 110 ppm, according to data [19], used in Ref. [13]. The temperature scenario is shown in Fig. 5a. External stresses were applied when the temperature reached 315 °C during cooling. The unique feature of these experiments was that the internal gas pressure was reduced during cooling and the rate varied in the range 0–10 bar/h. The corresponding history of circumferential stresses is shown in Fig. 5b.

As can be seen in Fig. 5, the stress is similar for all samples at high temperatures at the beginning of precipitation, but is significantly different at low temperatures. The cumulative RHF measured at the end of the experiment is an integral sum of hydrides precipitated at different time steps during cooling. Therefore, two approaches should predict a different dependence of the cumulative RHF on the decompression rate, since they assume a different dependence of the instantaneous f_r on stress and temperature: $f_{r1}(\sigma/T)$, according to Eq. (7) and $f_{r2}(\sigma)$, according to Eq. (12).

Fig. 6 shows the dependence of the RHF on the decompression rate in Ref. [13]. The experimental results for constant stresses ($dp/dt \sim 0$, test 7, [13]) have been used here to verify the "basic" models (Table 2). As a result, both "basic" models show good agreement with experimental data and with each other for slow decompression rates. However, the difference between the two "basic" models increases as the decompression rate increases. For a more precise analysis of the experimental and calculated dependencies of RHF on decompression rate, the slopes of the lines in Fig. 6a and b have been collected in Table 3.

According to Table 3, the slope of the line calculated by Approach 1 is a slightly lower and closer to the experimental value, than that calculated by Approach 2 for both quasi-static and diffusion approximations. This is because Approach 1 assumes the dependence of f_{r1} on σ/T. As a result, the reduction in stress during cooling is compensated to some extent by the reduction in temperature. Approach 2 assumes that f_{r2} depends only on σ, so it gives a smaller relative contribution of radially oriented hydrides precipitated at low temperatures and hence the sharper slope in Fig. 6. Note, that the only difference between the "basic" models is the dependence type of f_r function on stress and temperature and the calculated difference in Table 1 is a pure effect of the corresponding single assumption of the models.

Table 3
Parameters of the dependence of RHF on pressure reduction rate when cooling, which were determined by calculating the slopes of the lines shown in Fig. 6a and b.

[H], ppm	Slope (ΔRHF/$\Delta(dp/dt)$)				
	Experiment	Approach 1, "basic"		Approach 2, "basic"	
		quasi-static	diffusion	quasi-static	diffusion
100	1.14	1.86	1.65	2.01	2.00
150	1.09	1.20	0.94	1.52	1.12

The origin of the different slopes of the calculated lines in Fig. 6 can be better understood by looking at the instantaneous values of the calculated parameters. For fast decompression rate samples, the instantaneous f_{r2} decreases to zero when the stress becomes lower than the threshold, while f_{r1} is non-zero until the end of the test, as shown in Fig. 7a. For slow decompression rate specimens, the difference is even more significant. While in f_{r2} is a decreasing function proportional to the stresses, in f_{r1} increases during cooling due to the effect of temperature, as shown in Fig. 8a. The instantaneous precipitation rate of radially oriented hydrides on Fig. 7b and 8b has a smaller difference due to the fast exponential dependence of solubility on temperature, which minimizes the relative contribution of low temperatures. Nevertheless, it can be seen from Fig. 7b and 8b that Approach 2 overestimates the relative role of radial hydride precipitation at high temperatures and underestimates it at low temperatures compared to Approach 1. This is assumed here to be the main difference between the two kinetic approaches, which is a consequence of the different assumptions about the type of instantaneous f_r function. The calculated cumulative RHF (or F_r) may have different time dependencies, as shown in Fig. 7c and 8c, but the final values that can be compared with experimental values are similar under experimental conditions [22], and the difference is within the experimental uncertainty.

The diffusion approximation can give a more realistic simulation results, but the effect for the particular conditions is weak. It reduces the slope of the lines in Fig. 6a and b compared to the quasi-static approximation, as shown in Table 3. The first factor is that the diffusion approximation efficiently ''delays'' precipitation, thereby shifting precipitation to lower temperatures. The second factor is that at low temperatures the hydrogen diffusion coefficient is low, which increases the characteristic diffusion time τ_0. In the framework of the models used, this leads to a significant supersaturation remaining as a solid solution

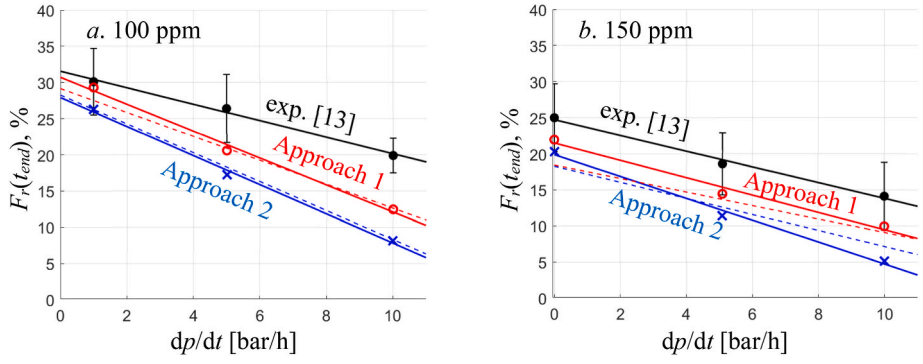

Fig. 6. Dependence of reoriented hydride fracture on the pressure reduction rate. black color and dots – experimental data by Ref. [13], red color and rings –Approach 1 ″basic", blue color and x – Approach 2 ″basic"; solid lines – experiments and quasi-static approx., dashed lines – diffusion approx.

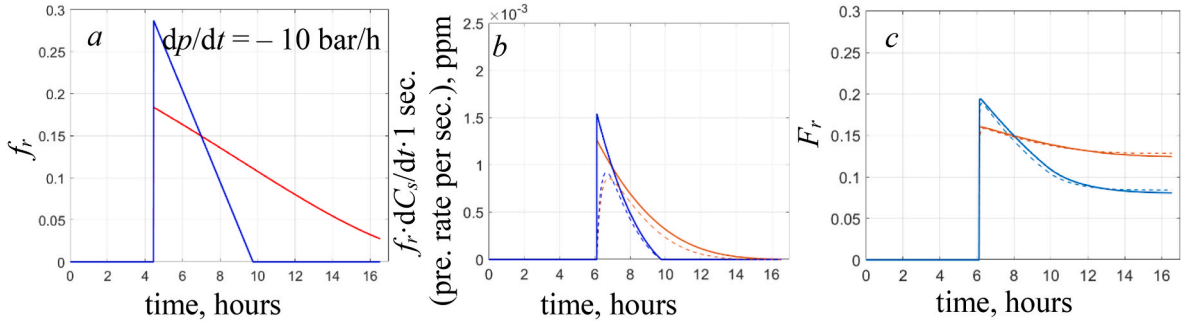

Fig. 7. F_r and radial hydride precipitation kinetics at "fast" stress reduction rate (10 bar/h); Test 3 in exp [13].: 98 ppm; red – Approach 1 ″basic", blue – Approach 2 ″basic"; solid lines – quasi static approx., dashed lines – diffusional approx.

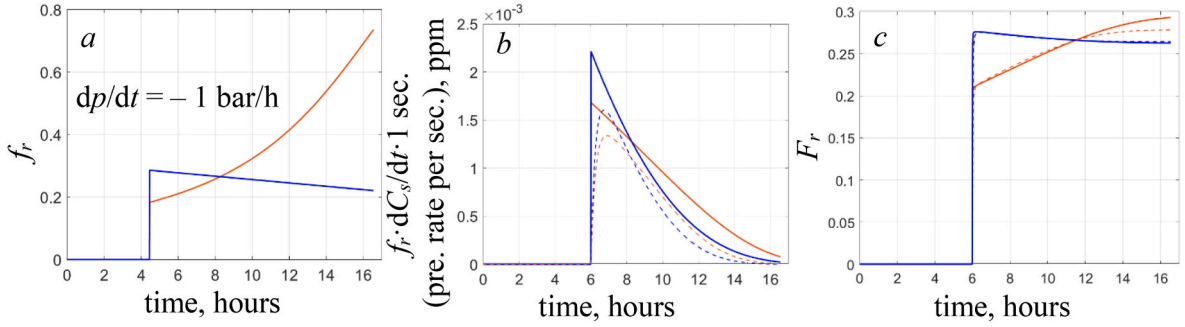

Fig. 8. F_r and radial hydride precipitation kinetics at "slow" stress reduction rate (1 bar/h); Test 3 in exp [13].: 98 ppm; red – Approach 1 ″basic", blue – Approach 2 ″basic", solid lines – quasi static approx., dashed lines – diffusional approx.

(up to ~ 20 ppm) after the experiment and reduces the total amount hydrogen precipitated as hydrides.

4.3. Comparison with experiments (summary)

Both approaches are able to simulate reorientation of hydrides after thermomechanical cycle with satisfactory accuracy, as it was demonstrated by comparison with the results of experiments (Figs. 2–4, 6a and 6b, Table 2). The more precise comparison with experiments according to Table 3 shows some evidence in favor of Approach 1 in the simulation of RHF in tests with changing stress during cooling. However, the difference in the slopes of the calculated curves on Fig. 6 is comparable to the uncertainty of the experimental data. Published experimental data can be described with acceptable accuracy under both assumptions.

The detailed analysis has shown that the two approaches interpret the role of temperature on hydride reorientation in a fundamentally different way, which is the consequence of different dependencies of f_r functions on temperature (Eq. (7) and Eq. (12)). For further investigation of hydride reorientation at low and high temperatures (i.e. the fraction of radially oriented hydrides precipitated after cooling for a small step dT at low and at high temperatures), additional experimental studies are required.

5. Other thermomechanical scenarios that could demonstrate differences in approaches

This section describes two thermomechanical scenarios where two approaches give different results. These discrepancies are due to the different dependencies of the F_r function on temperature assumed in the two approaches. Accordingly, the proposed scenarios are aimed at comparing the susceptibility to reorientation of hydrides precipitated at different temperatures. Both scenarios can be used in hydride reorientation experiments to evaluate and compare the efficacy of the two approaches, particularly under conditions where significant differentiation is anticipated.

In both scenarios the samples are assumed to be hydrogenated up to 240 ppm and then subjected to a thermocycle as shown in Fig. 5a. The temperature history is identical for both scenarios, with a cooling rate

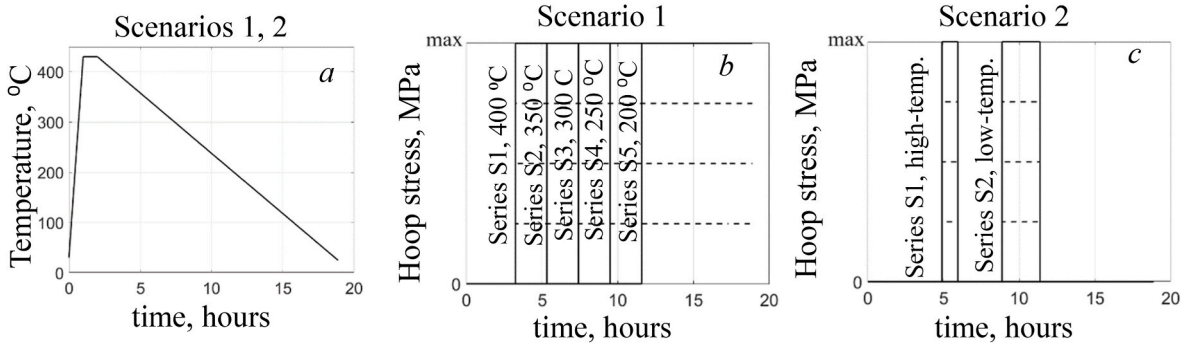

Fig. 9. Temperature and pressure history of thermomechanical Scenarios 1 and 2.

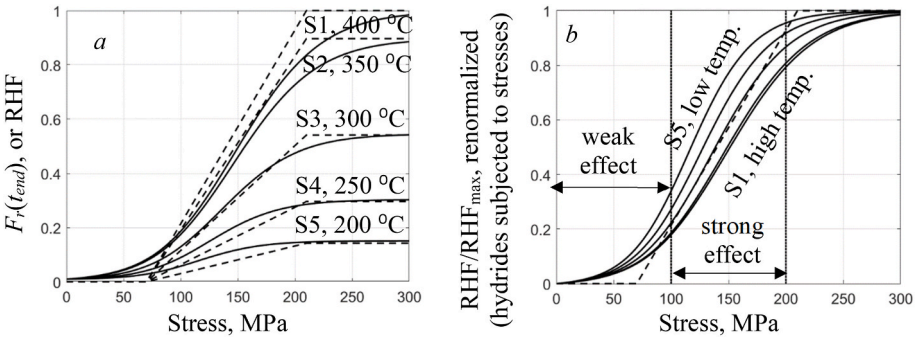

Fig. 10. Calculated RHF in Scenario 1. Pretests in quasi-static approximation; *a* – RHF of all hydrides; *b* – renormalized RHF (only hydrides subjected to reorientation) solid lines – Approach 1, dashed lines – Approach 2 (s1 – s5 give the same result).

1 °C/min and a maximum temperature of 430 °C, which allows for the complete dissolution of hydrides. The stress history is different in two scenarios and is shown in Fig. 9b and c. Pre-test calculations were carried out using quasi-static approximation of both approaches with parameters corresponding to Zircaloy-4.

5.1. Stress scenario 1

External stresses are applied during cooling when the temperature reaches a specific temperature and remains constant until the end of cooling. In Series 1, this temperature is 400 °C, in Series 2, it is 350 °C, and so on as shown in Fig. 9b. Each series must include at least five samples with five different constant stress levels to plot a reorientation curve for each series.

Fig. 10a illustrates the typical calculated reorientation curves, which encompass all hydrides present at the end of the test: precipitated prior to the application of external stresses (which are the majority for series with the temperature of applying stresses below 300 °C and containing almost all circumferential hydrides) and after (when the fraction of newly precipitated radial hydrides determined by the value of external stress). In order to investigate the reorientation process more precisely, it is necessary to distinguish the effect of stresses, which is blurred by the presence of parasitic hydrides that precipitated prior to the application of external stresses. To achieve this, it is proposed to renormalize the curves. Renormalization is based on considering only hydrides that may undergo reorientation and precipitate after applying external stress. The renormalized RHF can be found as:

$$\mathrm{RHF}_{renorm} = \frac{\mathrm{RHF}}{\max(\mathrm{RHF})} \tag{16}$$

As can be seen from Fig. 10b, Approach 2 predicts the same renormalized reorientation curve for each series, while Approach 1 predicts different ones. According to Approach 1, hydrides precipitated at low temperatures show a higher susceptibility to reorientation. The effect is weak at stresses below the lower threshold, but in the transition zone the difference between Series 1 and Series 5 is up to two times and can be detected in experiments.

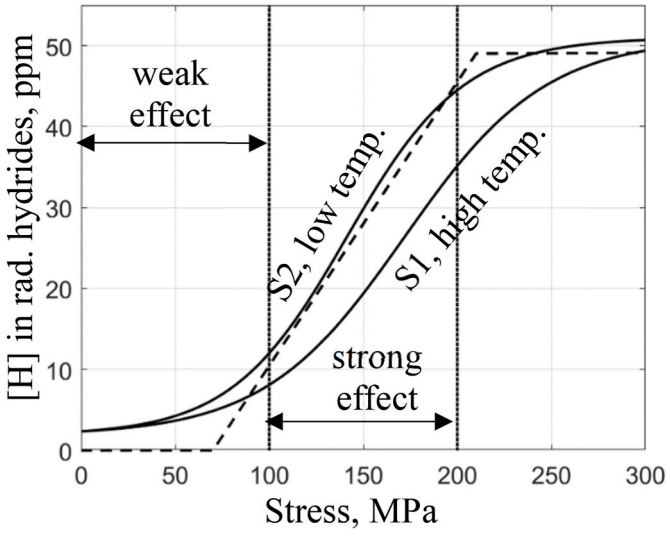

Fig. 11. Hydrogen content in radial hydrides after the Scenario 2. Pretests; solid lines – Approach 1, dashed lines – Approach 2 (S1 and S2 give the same results).

5.2. Stress scenario 2

The difference with Scenario 1 is that in Scenario 2 stresses are applied for a limited period of time during the cooling required to precipitate 50 ppm hydrogen. The corresponding temperature interval was determined according by TSSP from Ref. [20] as 360–335 °C (high temperature precipitation) and 265–205 °C (low temperature precipitation). The resultant stress history is shown in Fig. 9c.

Fig. 11 shows the concentration of hydrogen in radially oriented hydrides as a function of external stress, calculated from two approaches. Again, as in Scenario 1, Approach 2 gives identical reorientation curves for both series, whereas Approach 1 predicts distinct curves. According to Approach 1, the difference between high and low temperature precipitation in the transition zone at stresses between the thresholds can be significant and detectable in experiments. However, it should be noted that since the total hydrogen content in the samples was assumed to be 240 ppm, the maximum radial hydride fraction is only about 20 %.

5.3. Section summary

Approach 1 predicts that hydrides precipitated during cooling for a small temperature step dT at low temperatures are more susceptible to stress reorientation than hydrides precipitated at high temperatures, whereas Approach 2 assumes that the reorientation behavior is the same for different temperatures. Simulations above have shown that this difference in approaches is maximal at stresses between thresholds and can be detected in reorientation experiments. The main idea of each scenario is to split the stress induced precipitation of radial hydrides at low and high temperatures to investigate the influence of the instant temperature factor on the reorientation process. To improve the clarity of the experiments, it is desirable to achieve full hydride dissolution at the peak temperature, then, in accordance with this point, to maximize the hydrogen concentration in the samples (to broaden the temperature range in which low and high temperature nucleation are compared) and to maximize the stress range and minimize the stress step in order to plot the detailed and complete reorientation curve for each series of experiments.

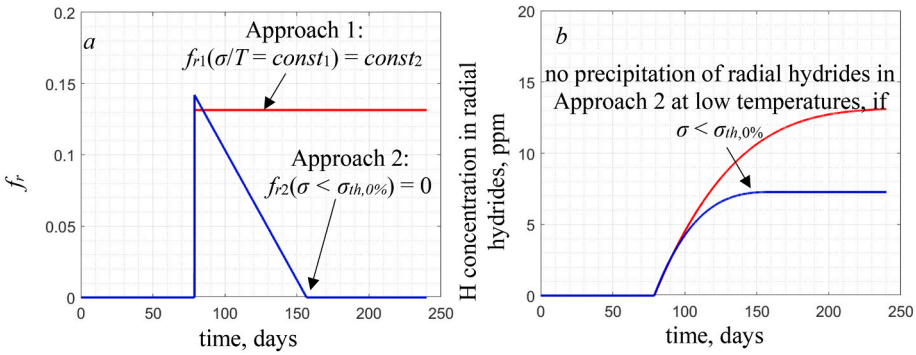

Fig. 12. Kinetics of radial hydride fraction precipitated at the current time step (left) and hydrogen concentration in radial hydrides (right) during slow cooling of sealed tubes loaded by internal gas pressure; red line – "basic" model of the Approach 1, blue line – "basic" model of the Approach 2.

6. Practical application consequences: dry storage conditions

Computational tools discussed above have been developed to simulate hydride orientation in cladding of fuel rods. The purpose of these tools is to predict the degree of hydride embrittlement of SNF cladding during DS and/or transport operations. All cases involve a thermocycling of sealed tubes with a constant amount of gas inside (in moles). In SNF DS conditions, the reduction in local temperature is accompanied by a reduction in stress, which is determined by the average temperature of the gas under the cladding. This differs from the majority of reorientation experiments, where the stresses are usually either held constant during cooling or reduced proportionally to temperature. Therefore, the hydride reorientation model must assume the correct and verified dependence of hydride orientation on stress and temperature.

Currently, two kinetic approaches assume different dependencies of the radial hydride fraction precipitated at a time step during cooling on stress and temperature. The consequence is a different assessment of the relative role of radial hydride precipitation at low temperatures, which is higher in Approach 1 compared to Approach 2 (can be seen in Fig. 7a and 8a). The consequences of different assumptions for simulations of DS conditions are shown in Fig. 12.

Fig. 12 shows the calculation results of a hypothetical experiment simulating dry storage conditions (close to the conditions of the SPIZWURZ experiment as described in Ref. [14]). The samples are sealed Zircaloy-4 tubes hydrogenated to 100 ppm and loaded by internal gas pressure with the constant amount of gas. They were heated to 400 °C and then slowly cooled to room temperature at a constant rate for 240 days. The hoop stresses are assumed to be equal to 110 MPa at 400 °C and then decrease proportionally with temperature, such that $\sigma/T = const_1$ as in a uniformly heated sealed tube. According to the assumptions of Approach 1, the instantaneous $f_{r1}(\sigma/T) = const_2$ at each time step under these conditions, as shown in Fig. 12a. In the assumptions of Approach 2, the kinetics of the instantaneous f_{r2} is significantly different; it is zero at low temperatures, as the hoop stress is less than the lower threshold. As a result, Approach 2 underestimates the hydrogen concentration in radial hydrides at low temperatures compared to Approach 1, as can be seen in Fig. 12b. While the absolute values in the simulated conditions do not differ significantly, there is a marked divergence in the understanding of the relative role in the reorientation process of radial hydride precipitation at low temperatures.

7. Conclusion

Currently, there are two popular kinetic approaches for modelling the radial hydride fraction in SNF rod cladding. Both approaches are able to simulate the reorientation of hydrides after the typical thermomechanical cycle with satisfactory accuracy. However, the dependencies of the instantaneous radial hydride fraction f_r on stress and temperature is different in the two approaches, because they are based on different assumptions. As a result, Approach 2 may underestimate the relative role of low temperature precipitation of radially oriented hydrides compared to Approach 1. This can lead to a different understanding of low temperature precipitation and different calculated precipitation kinetics of hydrides under SNF DS conditions. Two thermomechanical scenarios that can be used to experimentally investigate the dependence of the f_r function on stress and temperature are suggested.

Declaration of competing interest

The authors declare the following financial interests/personal relationships which may be considered as potential competing interests: The author declares that he is a co-author of a certified model based on the assumptions relevant to Approach 1 in this paper.

References

[1] A.T. Motta, et al., Hydrogen in zirconium alloys: a review, J. Nucl. Mater. 518 (2019) 440–460, https://doi.org/10.1016/j.jnucmat.2019.02.042.
[2] M. Kolesnik, Micro-mechanisms of the ductile-to-brittle transition in hydrogenated zirconium alloys: a review and a comparison analysis of experimental data and theo- retical approaches, Eng. Fail. Anal. (2024) 108110, https://doi.org/10.1016/j.engfailanal.2024.108110.
[3] W. Xufeng, et al., Effect of process variables on texture and hydride orientation of cold pilgered Zr-Sn-Nb-Fe cladding tubes, J. Mater. Eng. Perform. (Ref 10) (2023), https://doi.org/10.1007/s11665-023-09006-w.
[4] J. Li, et al., Effect of hydride precipitation on the fatigue cracking behavior in a zirconium alloy cladding tube, Int. J. Fatig. 129 (2019) 105230, https://doi.org/10.1016/j.ijfatigue.2019.105230.
[5] C.E. Ells, The stress orientation of hydride in zirconium alloys, J. Nucl. Mater. 35 (3) (1970) 306–315, https://doi.org/10.1016/0022-3115(70)90214-X.
[6] D. Hardie, M.W. Shanahan, Stress reorientation of hydrides in zirconium-2.5% niobium, J. Nucl. Mater. 55 (1) (1975) 1–13, https://doi.org/10.1016/0022-3115(75)90132-4.
[7] J.B. Bai, N. Ji, D. Gilbon, C. Prioul, D. François, Hydride embrittlement in ZIRCALOY-4 plate: Part II. interaction between the tensile stress and the hydride morphology, Metall. Mater. Trans. A 25 (6) (1994) 1199–1208, https://doi.org/10.1007/BF02652294.
[8] J. Desquines, et al., Influence of temperature and hydrogen content on stress-induced radial hydride precipitation in Zircaloy-4 cladding, J. Nucl. Mater. 453 (2014) 131–150, https://doi.org/10.1016/j.jnucmat.2014.06.049.
[9] J. Li, Z. Wang, H. Wu, G. Chen, Microstructural and crystallographic analysis of hydride reorientation in a zirconium alloy cladding tube, J. Nucl. Mater. 537 (2020) 152232, https://doi.org/10.1016/j.jnucmat.2020.152232.
[10] M. Kolesnik, T. Aliev, V. Likhanskii, Modeling of hydrogen behavior in spent fuel claddings during dry storage, J. Nucl. Mater. 508 (2018) 567–573, https://doi.org/10.1016/j.jnucmat.2018.06.012.
[11] M. Kolesnik, T. Aliev, V. Likhanskii, Modeling of size, aspect ratio, and orientation of flattened precipitates in the context of Zr-H system under external stress, Comput. Mater. Sci. 189 (2021) 110260, https://doi.org/10.1016/j.commatsci.2020.110260.
[12] A.R. Massih, L.O. Jernkvist, Stress orientation of second-phase in alloys: hydrides in zirconium alloys, Comput. Mater. Sci. 46 (4) (2009) 1091–1097, https://doi.org/10.1016/j.commatsci.2009.05.025.
[13] J. Desquines, C. Sartoris, M. Guémas, A. Gérard, Radial hydride precipitation in fuel cladding during back-end cooling transient under decreasing pressure, in: Water Reactor Fuel Performance Meeting, WRFPM 2023, 2023, pp. 80–86, https://doi.org/10.1007/978-981-99-7157-2_8.

[14] M. Grosse, et al., The SPIZWURZ project – experimental investigations and modeling of the behavior of hydrogen in zirconium alloys under long-term dry storage conditions, Nucl. Eng. Technol. 56 (2024) 824–831, https://doi.org/10.1016/j.net.2023.09.027.
[15] F. Feria, C. Aguado, L.E. Herranz, Extension of FRAPCON-xt to hydride radial reorientation in dry storage, Ann. Nucl. Energy 145 (2020) 107559, https://doi.org/10.1016/j.anucene.2020.107559.
[16] P. Konarski, C. Cozzo, G. Khvostov, H. Ferroukhi, Development and testing of the hydrogen behavior tool for Falcon – hype, Nucl. Eng. Technol. 56 (2) (2024) 728–744, https://doi.org/10.1016/j.net.2023.11.012.
[17] H.C. Chu, S.K. Wu, R.C. Kuo, Hydride reorientation in Zircaloy-4 cladding, J. Nucl. Mater. 373 (1–3) (2008) 319–327, https://doi.org/10.1016/j.jnucmat.2007.06.012.
[18] Q. Auzoux, et al., Hydride reorientation and its impact on mechanical properties of high burn-up and unirradiated cold-worked stress-relieved Zircaloy-4 and ZirloTM fuel cladding, J. Nucl. Mater. 494 (2022) 153893, https://doi.org/10.1016/j.jnucmat.2022.153893.
[19] K. Une, S. Ishimoto, Dissolution and precipitation behavior of hydrides in Zircaloy-2 and high Fe Zircaloy, J. Nucl. Mater. 322 (1) (2003) 66–72, https://doi.org/10.1016/S0022-3115(03)00320-9.
[20] G.F. Slattery, The terminal solubility of hydrogen in zirconium alloys between 30 and 400 C, J. Inst. Met. 95 (1967).
[21] W.H. Erickson, D. Hardie, The influence of alloying elements on the terminal solubility of hydrogen in α-zirconium, J. Nucl. Mater. 13 (2) (1964) 254–262, https://doi.org/10.1016/0022-3115(64)90046-7.
[22] Z.L. Pan, I.G. Ritchie, M.P. Puls, The terminal solid solubility of hydrogen and deuterium in Zr-2.5Nb alloys, J. Nucl. Mater. 228 (2) (1996) 227–237, https://doi.org/10.1016/S0022-3115(95)00217-0.
[23] J.J. Kearns, Diffusion coefficient of hydrogen in alpha zirconium, zircaloy-2 and zircaloy-4, J. Nucl. Mater. 43 (3) (1972) 330–338, https://doi.org/10.1016/0022-3115(72)90065-7.